DOI:10.1093/jnci/djt226

ARTICLE

Pleiotropic Effects of the Trichloroethylene-Associated P81S *VHL* Mutation on Metabolism, Apoptosis, and ATM-Mediated DNA Damage Response

Michelle C. DeSimone, W. Kimryn Rathmell, David W. Threadgill

Manuscript received December 7, 2012; revised July 7, 2013; accepted July 18, 2013.

Correspondence to: David W. Threadgill, PhD, Departments of Veterinary Pathobiology and Molecular & Cellular Medicine, 440 Reynolds Medical Bldg, College Station, TX 77843-1114 (e-mail: dwthreadgill@cvm.tamu.edu).

Background The risk relevance of the P81S von Hippel-Lindau (VHL) gene hotspot mutation identified in clear cell renal cell carcinoma from individuals exposed occupationally to trichloroethylene (TCE) is not known. *VHL* mutations in hereditary VHL syndrome strongly correlate with phenotypic associations, but specific sporadic mutations in *VHL* that uniquely alter its protein function may provide a selective growth advantage for somatic cells harboring these mutations.

Methods VHL deficient ($Vhl^{-/-}$) mouse embryonic stem cells were generated that stably express wild-type, P81S, or R167Q human VHL protein. Under hypoxic conditions, cell lines were examined for hypoxia-inducible transcription factor family (HIF) stabilization and E3-ubiquitin ligase complex interactions. In vivo, teratomas were examined for tumor size, proliferation, apoptosis, and immunohistochemistry and subjected to gene expression analysis. Wild-type, R167Q, and P81S VHL-expressing teratomas were also exposed to 5 Gy ionizing radiation to quantify apoptotic response. Proliferation and apoptosis and teratoma growth were analyzed by either Student *t* test or analysis of variance with Bonferroni correction. All statistical tests were two-sided.

Results The P81S *VHL* mutation produces deregulation of HIF factors in cell culture but exhibits a growth advantage in the tumor microenvironment, in part because of suppression of apoptosis (P81S mean = 0.9%, 95% confidence interval = 0.6 to 1.2%; WT mean = 7.6%; 95% confidence interval = 6.4 to 8.8%; $P < .001$) coupled with sustained proliferation. Transcriptional analysis of P81S teratomas revealed the induction of metabolic pathways, antiapoptotic genes, and global suppression of key DNA damage response genes not observed in *VHL* wild-type or R167Q mutants. In vivo irradiation exposure showed that P81S mutant is resistant to ionizing radiation–induced apoptosis.

Conclusions The TCE-associated P81S *VHL* mutation can initiate a unique adaptive response required for selective tumor growth through pleiotropic effects on metabolic diversification, apoptosis suppression, and alteration of the DNA damage response.

J Natl Cancer Inst;2013;105:1355–1364

Epidemiological studies have linked exposure to trichloroethylene (TCE), an organic solvent classified as a group 1 carcinogen and recognized contaminant in groundwater, with increased incidences of clear cell renal cell carcinoma (ccRCC). A tumor-specific somatic *C454T* missense mutation in the von Hippel-Lindau tumor suppressor gene (*VHL)* has been linked with TCE-associated ccRCC cases (1,2). This mutation results in a single amino acid change from proline to serine at codon 81 of the VHL protein (P81S) and is observed in more than 39% of TCE-exposed individuals who developed ccRCC (1).

The VHL tumor suppressor functions as a redox sensor, controlling stability of the hypoxia-inducible transcription factor family (HIFs). VHL forms a complex with Elongin B (TCEB2), Elongin C (TCEB1), Ringbox1 (RBX1), and Cullin2 (CUL2) to form an E3 ubiquitin ligase complex (VBC complex) (3). Under normal oxygen conditions, oxygen-dependent prolyl-hydroxylase (PHD) enzymes hydroxylate HIF proteins at two specific proline residues that are recognized by VHL, and the VBC complex then polyubiquitinates HIF for degradation by the 26S proteasome (4). Cancer-associated missense mutations in *VHL* disrupt its function in the E3 ubiquitin ligase complex, resulting in variable deregulation of HIF factors (5,6). Structural models of molecular interactions between VHL and TCEB1 showed codons 81 and 82 of VHL are direct TCEB1 binding sites, suggesting that the P81S mutation associated with TCE exposure could destabilize the VBC complex and result in HIF-mediated transcriptional activation of hypoxia response targets (7).

The HIF family members (HIF1A and HIF2A) play a central role in metabolic reprogramming observed in human renal tumors, which is thought to provide a selective survival advantage in changing microenvironments by modifying energy use during periods of hypoxic and glycolytic stress (8). This diversification of energy

sources through increased glycolysis (the Warburg Effect) (9), fatty acid oxidation (10,11), and glutaminolysis (12–14) can promote cell proliferation and, in some cases, resistance to chemotherapeutic-induced apoptosis (15). HIF activation and metabolic changes have also been implicated as a result of Ataxia Telangiectasia Mutated (ATM) activation, a protein kinase involved in the response to DNA damage (16,17). Although HIF activation suggests a possible link between ATM-mediated DNA damage response and VHL, this has not been previously detected.

In this study, the TCE-associated P81S VHL mutation was modeled and its activity compared with cells expressing normal VHL and the hotspot R167Q VHL mutant that was previously shown to dysregulate both HIF factors in graded fashion (5,6,18). The results show that the unique TCE-associated *VHL* mutation has pleiotropic effects that selectively influence the tumor behavior in a mutation-specific manner, providing a selective growth advantage through metabolic diversification, apoptosis suppression, and alteration of the DNA damage response.

Methods

Site-Directed Mutagenesis

Vhl$^{-/-}$ embryonic stem (ES) cells were generated and propagated as previously described (18). Site-directed mutagenesis of the pST-HA-*VHL* parental construct to mutate the proline at nucleotide position 454 to a serine residue was performed using the QuikChange II XL site-directed mutagenesis kit (Stratagene, La Jolla, CA). Primer sets used were (specific base changes underlined) 5′-GCAATCGCAGT*T* CGCGCGTCG-3′ and 5′-CGACGCGCG*A*ACTGCGATTGC-3′. ES clones were selected using media containing 200 μM hygromycin and were tested for hemaggulutinin (HA)–VHL expression by Western blot. Immunoprecipitation experiments were performed using the Pierce Mammalian HA-tag Co-IP kit (Pierce, Rockford, IL) as previously described (5).

Hypoxia Treatments

ES cell lines were plated on gelatin-coated cell culture dishes and exposed to 100 uM cobalt (II) chloride ($CoCl_2$), a hypoxia mimetic, for 16 hours, whereas normoxic controls received media replacement only. After treatment, cell pellets were isolated and snap frozen for RNA isolation or Western blot analysis. Western blots were performed as previously described (5), and blot densitometry was performed using ImageJ software (http://imagej.nih.gov/ij/).

In Vivo Teratomas and Reverse-Transcription Polymerase Chain Reaction (RT-PCR)

Female *Foxn1*$^{nu/nu}$ mice aged 6 to 8 weeks were injected subcutaneously in bilateral flanks with 1×10^6 cells of each HA-VHL cell line, for a total of eight tumors (two per mouse) per wild-type (WT) and R167Q clone and 16 total for two independent P81S clones. Tumor growth was measured three times a week using calipers until tumors reached a maximum dimension of 1 cm. To examine tumor hypoxia, mice were injected with 60 mg/kg Hypoxyprobe-1 (Natural Pharmacia International, Belmont, MA) 1 hour before they were killed. Tumors were excised and either flash frozen or formalin-fixed and paraffin-embedded. Total RNA from teratomas and ES cell pellets was isolated using RNAeasy Mini Kits (Qiagen, Valencia, CA), followed by cDNA preparation from 10 to 40 ng/uL RNA using Applied Biosystems (Carlsbad, CA) cDNA Archive kit. For quantitative RT-PCR, primer/probe sets were purchased from Applied Biosystems. Data were normalized to loading control beta-glucuronidase or beta-actin, and results were calculated using the ΔΔCt method (19). Animal studies were approved by the Institutional Animal Care and Use Committee.

Radiation Exposure

Teratomas were grown as above, and mice were placed into a Gammacell 40 Exactor CS-137 irradiator (Best Theratronics, Ottawa, Ontario) with a radiation source of 1800 ± 15% Curies (Ci) cesium 137 and delivered a single dose of 5 Grays (Gy), whereas others received no treatment. Mice were killed 4 and 24 hours after exposure, and tumors were formalin fixed and paraffin embedded.

Immunohistochemistry and Microarray Analysis

Immunohistochemistry was performed on 5-μm paraffin-embedded sections using the following primary antibodies: anti-Ki67 and anti-cyclin D1 (Abcam, Cambridge, MA); anti-hypoxyprobe-1 (Hypoxyprobe, Inc); and anti-phosphorylated ATM at Serine 1981 (Sigma-Aldrich, St. Louis, MO). Avidin-biotin complex (ABC) enhancement kit and 3,3′-diaminobenzidine (DAB) detection reagent (Vector Laboratories, Burlingame, CA) was used for visualization. Apoptosis staining was performed using the ApopTag In Situ Apoptosis Detection Kit (Millipore, Billerica, MA). Slides were counterstained with 2-(4-amidinophenyl)-1H-indole-6-carboxamidine (DAPI) to facilitate cell counts. Quantitative analysis was performed using BIOQUANT software (BIOQUANT Image Analysis, San Diego, CA) by averaging percentage of positively stained cells to total cells within six random fields at ×200 magnification. Microarray experiments were performed using GeneChip Mouse ST Gene 1.1 whole genome arrays (Affymetrix, Santa Clara, CA) at the University of North Carolina Genomics Core Facility. The data have been deposited in the National Center for Biotechnology Information's Gene Expression Omnibus (20) and are accessible through accession number GSE37464.

Pathway and Statistical Analysis

Gene expression data (CEL files) were analyzed using Partek Genomic Suite, version 6.5 (Partek Inc, St. Louis, MO). Gene expression data were normalized by robust multiarray analysis, and analysis of variance (ANOVA) was performed using Partek software. Differentially expressed genes were identified between classes using the nonparametric rank-product method ($P < .05$ and $P < .01$), and $\log_2$ expression values for each gene were generated. Canonical pathway analysis was generated through the use of Ingenuity Pathways Analysis (Ingenuity Systems, Redwood City, CA). Canonical pathway analysis was measured as a ratio of the number of genes from the dataset that map to a pathway divided by the total number of genes that map to the canonical pathway. Fisher exact test was used to calculate a *P* value. Significance for real-time RT-PCR experiments, quantification of proliferation and apoptosis, and teratoma growth was determined by either Student *t* test for comparison of two groups or ANOVA with Bonferroni correction for significance comparing VHL mutants with WT VHL. All statistical tests were two-sided.

Results

To test whether the P81S VHL mutant disrupts VBC complex interactions, extracts from *VHL* deficient (*Vhl*$^{-/-}$) murine ES cells expressing HA-tagged WT, P81S, or R167Q human VHL protein were immunoprecipitated with an antibody directed toward the HA tag and examined for coimmunoprecipitation with VBC complex members. WT VHL cells retained their interaction with all VBC complex members, However, extracts from both P81S and R167Q mutants failed to coprecipitate with TCEB1 (Elongin C [Figure 1A]) but did retain interaction with CUL2 (Culin 2), RBX1 (Ringbox 1), and TCEB2 (Elongin B) (Figure 1, A and B).

Disruption of the VBC complex would result in loss of HIF targeting and lead to stabilization of HIF during normal oxygen conditions. To evaluate HIF levels, two independent clones of the P81S mutant, as well as *Vhl*$^{-/-}$, WT, and R167Q cell lines, were analyzed for HIF1A protein expression after 16 hours of growth in the presence of normal oxygen (21% O_2) or hypoxia mimetic $CoCl_2$ (Figure 1C). HIF1A was stabilized under normoxic conditions with no further increase during treatment with $CoCl_2$ in *Vhl*$^{-/-}$ cells, whereas HIF1A protein was minimal in lysates from WT VHL cells in normoxic conditions, suggesting degradation of HIF by the VBC complex. In contrast, HIF1A remained partially stabilized in P81S and R167Q mutant cells during normoxia, consistent with the inability of VHL mutants to support normal VBC complex function.

To verify that stabilized HIF1A protein results in functional activity, transcriptional activation of HIF-targeted genes was quantified by RT-PCR using mRNA isolated from P81S, WT, R167Q, and *Vhl*$^{-/-}$ cell lines (Figure 1D). Whereas R167Q showed greater than twofold excess transcript levels compared with WT for HIF1A target genes *EglN3* and *Vegf* during normoxia with further induction during hypoxia, *Glut1* was regulated normally in these conditions. In contrast, P81S displayed a normoxic excess of the glucose transporter *Glut1* but normal regulation of the targets *EglN3* and *Vegf*, suggesting differential HIF1A targeting occurs between the R167Q and P81S *VHL* mutants. The most notable difference observed between the mutants and the *Vhl*-deficient cells was in the degree to which HIF1A was stabilized. Both P81S and R167Q mutants preserved the ability of hypoxia to induce HIF1A beyond basal levels, suggesting that neither mutant produced maximal stabilization of HIF.

During a physiological response to hypoxia, HIF factors are stabilized to activate the expression of hypoxia response element (HRE)-dependent genes, which represent a wide range of physiological processes, including angiogenesis, energy metabolism, glycolysis, and cell cycle (4,21). In addition to physiological processes, another major limitation of examining cell lines in vitro is the inability to examine deregulated HIF2 transcriptional activity (18,21). Therefore, to study the phenotypic consequences under conditions mimicking the tumor environment, ES cell lines were subcutaneously injected in the flank region of nude mice to evaluate in vivo teratocarcinoma growth. The most striking effect was a threefold increase in P81S teratoma volume relative to WT and a sixfold increase over R167Q teratomas (Figure 2, A–C). *Vhl*$^{-/-}$ cells were nearly completely impaired in supporting teratoma growth (data not shown). The relative proliferation index between WT and P81S teratomas was not statistically significantly different (Figure 2, E and F), suggesting that a proliferative advantage was not the primary reason for increased teratoma volume. Rather, results showed a statistically significant reduction in the percentage of apoptotic cells in P81S compared with both WT and R167Q (P81S mean = 0.9%, 95% confidence interval [CI] = 0.6% to 1.2% vs WT mean = 7.6, 95% confidence interval = 6.4% - 8.8%; $P < .001$) (Figure 2, G and H).

Analysis of teratoma sections revealed disorganized vascularization in the R167Q teratomas consistent with sustained HIF response (Figure 2D). P81S teratomas, in contrast, displayed an increase in microvessel density but overall a pattern more consistent with WT teratomas. Because tumor vasculature can modify oxygen delivery and apoptotic response, hypoxia was analyzed using a hypoxia tracer (Figure 2I). The R167Q mutant demonstrated global reduction in regional hypoxia, whereas no differences were observed between WT and P81S, suggesting that the growth advantage associated with the P81S mutation does not result from an angiogenic response.

Because analysis of in vitro grown cells suggested VHL mutants show differential HIF1A regulation (Figure 1D), expression of the HIF2A target gene Cyclin D1 (CCDN1) was analyzed. CCDN1 was overexpressed specifically in P81S teratomas (Figure 2J), further suggesting differential HIF isoform deregulation between the two mutants may be driving phenotypic differences. Because of the numerous HIF targets as well as stress response genes that may contribute to phenotypic differences, gene expression profiling of RNA from VHL teratomas was used to elucidate molecular pathways underlying the unique P81S adaptive response.

Unsupervised hierarchical clustering of whole genome microarray data showed independent clustering of replicate P81S teratomas distinct from WT and R167Q teratomas. Analysis of variance of all genes revealed that samples segregated based on genotype, with the WT and R167Q teratomas appearing more similar to each other than to the P81S teratomas, with 2622 genes differentially expressed among the three genotypes (Figure 3A). RT-PCR validation of select differentially expressed genes was performed (Figure 4). Pathway analysis of gene sets differentially expressed in WT vs both mutant genotypes revealed several functional differences consistent with VHL-associated phenotypes (Figure 5).

Biological pathway analysis on all statistically significantly expressed genes ($P < .05$) identified molecular pathways uniquely expressed in the P81S mutant, including modulation of HIF-specific targets, indicative of redirected HIF targeting (Figure 3B). P81S teratomas also had increased expression of genes associated with energy metabolism, including fatty acid oxidation, mitochondrial biogenesis, and glutaminolysis, suggestive of the use of glutamine-derived α-ketogluterate for energy production. Mitochondrial respiration has been shown to be essential for tumor proliferation (12,13), suggesting that alternative use of lipids and glutamate as a source of acetyl coenzyme A may be an important adaptive mechanism in P81S teratomas. Mitochondrial metabolism increases the production of reactive oxygen species and, as a consequence, induces genes associated with antioxidant activity (22,23), which was also observed in the P81S teratomas.

Cancer cells often upregulate an intrinsic stress response system during tumor hypoxia or oxidative stress to avoid apoptotic signals (24,25). In agreement, the antiapoptotic gene *Bcl2* was upregulated

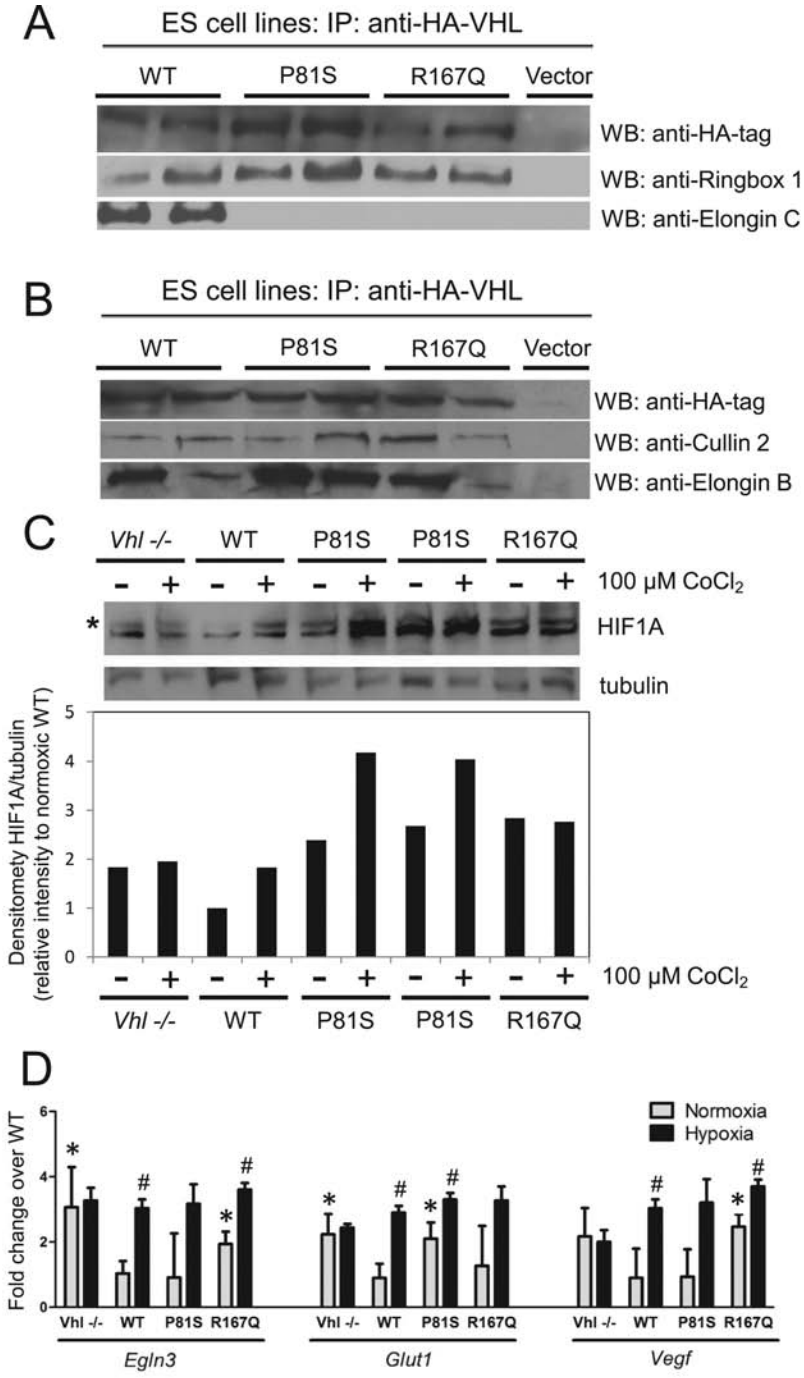

Figure 1. *VHL* mutants partially abrogate VBC complex interactions and allow hypoxia-inducible transcription factor family (HIF) transactivation during normal oxygen conditions. Immunoprecipitation of stably transfected *Vhl*$^{-/-}$ mouse embryonic stem (ES) cell lines expressing hemaggulutinin (HA)–tagged wild-type (WT), two independent clones of P81S mutant or R167Q mutant *VHL* under normoxic conditions. Cells were lysed under nondenaturing conditions and subject to coimmunoprecipitation with an antibody against the HA tag. Anti-HA precipitated products were probed for pull-down of HA-VHL with VBC complex members Ringbox 1 and Elongin C (**A**) and Cullin 2 and Elongin B (**B**). **C**) Immunoblot of HIF1A stabilization during normoxic and hypoxic conditions. Whole-cell protein extracts were prepared from stably transfected *Vhl*$^{-/-}$ mouse ES cells expressing WT, P81S mutants, or R167Q mutant HA-VHL under normoxic and hypoxic conditions induced by 100 μM cobalt (II) chloride ($CoCl_2$). Western blot shows HIF1A. * denotes HIF1A protein as the upper band. Beta-tubulin was loading control. Densitometric analysis using ImageJ software of HIF1A/tubulin is shown with relative intensity to normoxic WT. **D**) Expression of HIF1A transcriptional target genes in VHL ES cell lines grown under normoxic and hypoxic conditions for 24 hours. The expression was examined by reverse-transcription polymerase chain reaction. Beta-actin was used as the loading control. Data are mean fold expression over normoxic WT ± 95% confidence intervals of three independent cultures from two independent experiments. *P* values were calculated using two-sided Student *t* test. *$P \leq .01$ relative to normoxic WT. #$P \leq 0.04$ relative to normoxic treatment of same cell line. *Vegf* = vascular endothelial growth factor alpha; *Glut1* = glucose transporter 1; *Egln3* = elongin 3; IP, immunoprecipitation; WB, western blot.

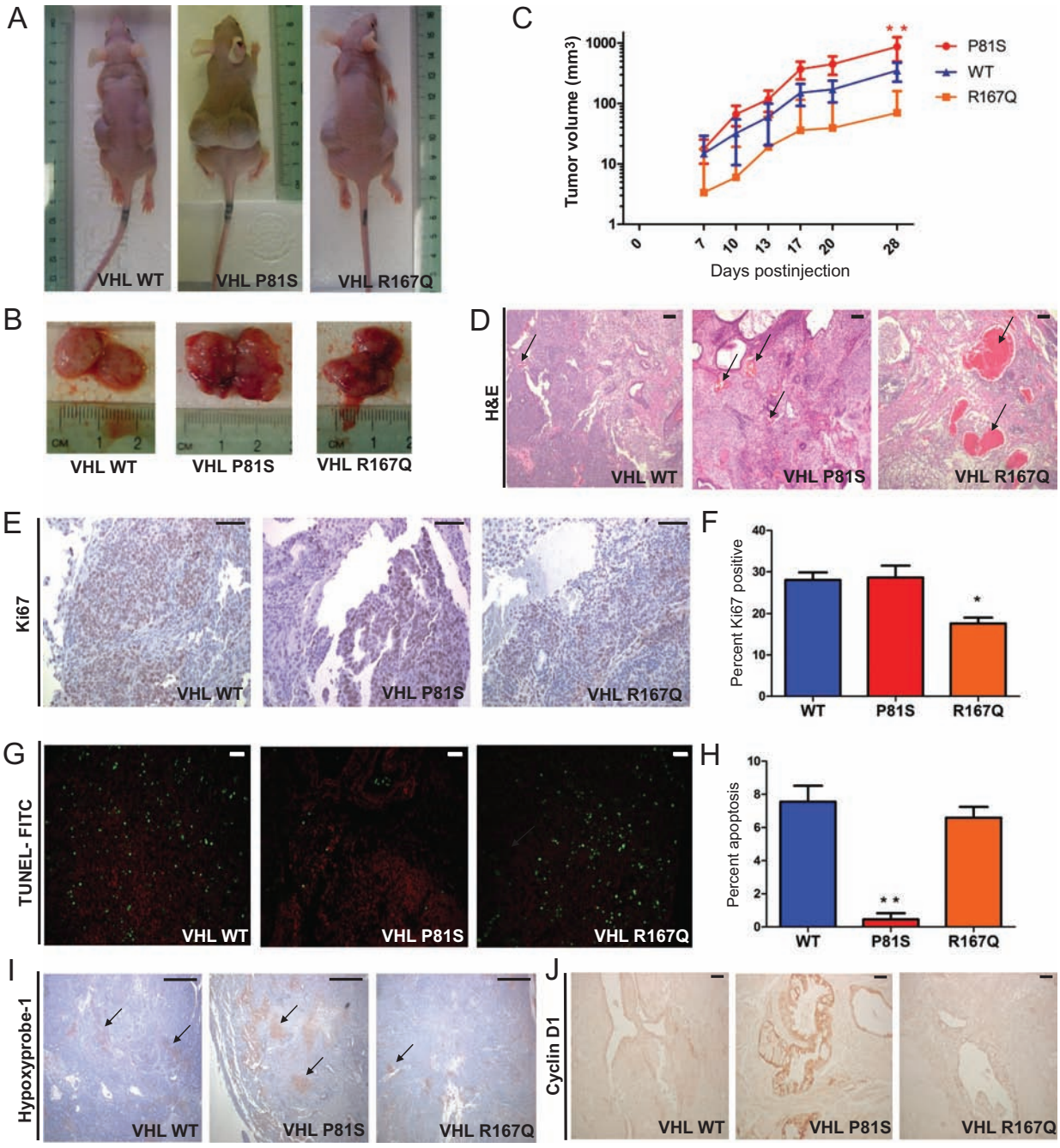

Figure 2. The P81S VHL mutant displays a marked growth advantage and apoptotic resistance despite hypoxic tumor microenvironment. **A**) In vivo teratoma assay of VHL embryonic stem (ES) cell clones. Stably transfected *Vhl*$^{-/-}$ mouse ES cells expressing wild-type (WT), two independent clones of P81S or R167Q VHL were injected subcutaneously into the flank region of nude mice and allowed to grow for 4 weeks. Mice were killed, and teratomas were removed and photographed. **B**) Gross images of ES cell teratomas bisected to visualize blood vessels and placed next to a standard metric ruler for size reference. **C**) Tumor volume was measured weekly using calipers. Data are mean tumor volume ± 95% confidence interval of eight individual tumors per VHL clone, including two P81S clones. *P* values were calculated at 4 weeks using analysis of variance with Bonferroni correction. $^{**}P \leq .001$ comparing P81S and R167Q with WT. **D**) Hematoxylin and eosin (H&E) staining of WT, P81S, and R167Q VHL teratoma sections show areas of differentiation and neovascularization, as indicated by **black arrows**. Scale bars = 100 μm. **E**) Immunohistochemistry for the proliferation marker Ki67 was performed on paraffin-embedded 5-μM sections showing positively stained cells in **brown**. Scale bars = 100 μm. **F**) Quantification of proliferation was performed by averaging percentage of positively stained cells to total cells within six random fields at ×200 magnification. Data show mean percentage ± 95% confidence interval of eight individual tumors per VHL clone. Statistical significance was determined by analysis of variance with Bonferroni correction. $^{*}P \leq .008$ comparing P81S and R167Q with WT. **G**) Immunohistochemical analysis of apoptosis using a modified terminal deoxynucleotidyl transferase dUTP nick end labeling (TUNEL-FITC) assay with fluorescein isothiocyanate detection on paraffin-embedded 5-μM sections. **Red**: DAPI nuclear stain; **Green**: cells positive for apoptosis. Scale bars = 100 μm. **H**) Quantification of apoptosis was performed by averaging percentage of positively stained cells to total cells within six random fields at ×200 magnification. Data show mean percentage ± 95% confidence interval of eight individual tumors per VHL clone. Statistical significance was determined by analysis of variance with Bonferroni correction. $^{**}P \leq .001$ comparing P81S and R167Q with WT. **I**) Immunohistochemical analysis of tumor sections for hypoxic regions using hypoxyprobe-1. **Black arrows** denote areas positively stained for hypoxia. Scale bars = 500 μm. **J**) Immunohistochemistry for HIF2A target, cyclin D1, was performed on paraffin-embedded 5-μM sections showing increased cyclin D1 expression in P81S teratomas. Scale bars = 100 μm.

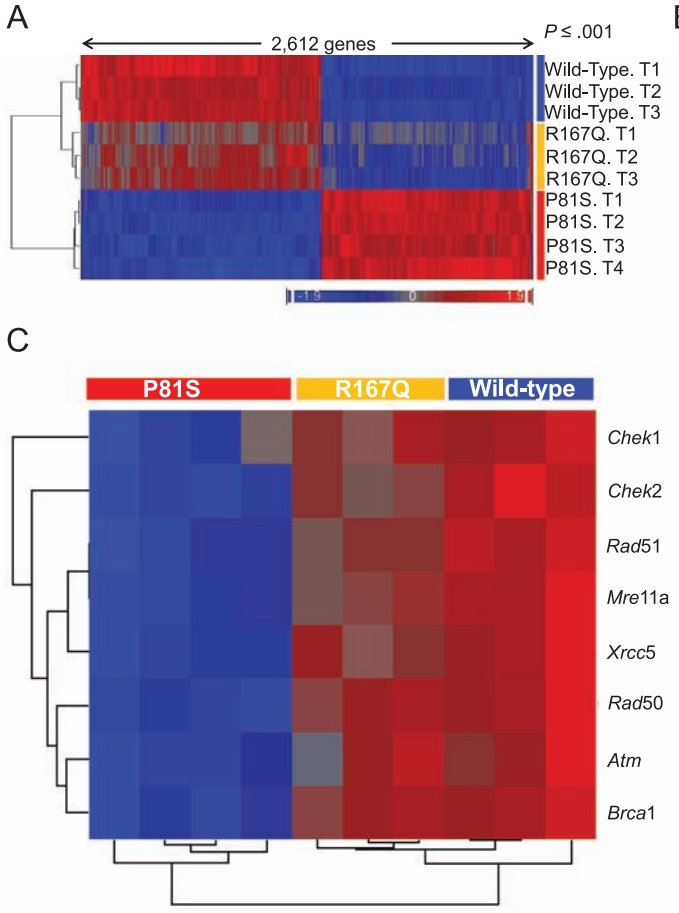

B

Genes enriched exclusively in *VHL* P81S teratomas

Metabolism: Fatty Acid, Beta-Oxidation, Glutaminolysis

Gene symbol	Gene name	Fold change	*P* value
Cpt1c	Carnitine palmitoyltransferase	1.36	.033
Crat	Carnitine acetyltransferase	1.38	.00067
Acsbg1	Acyl-CoA synthetase bubblegum family member 1	2.19	.0015
Acot11	Acyl-CoA thioesterase 11	1.65	.0044
Acsl6	Acyl-CoA synthetase long-chain family member	1.93	.0092
Acox1	Acyl-Coenzyme A oxidase 1, palmitoyl	1.48	.0074
Acox2	Acyl-Coenzyme A oxidase 2	1.68	.02
Glul	Glutamate-ammonia ligase, glutamine synthetase	1.17	.0017

Mitochondrial Biogenesis

Gene symbol	Gene name	Fold change	*P* value
Ppargc1a	Peroxisome proliferator activated receptor γ, c1a	2.62	.00005
Rab3a	RAB3A, member Ras oncogene	3.07	5.0E-06
Gnas	Gnas	1.21	.0029
Dnaja6	Hsp40	2.85	9.0E-07
Ldhd	Lactate dehydrogenase	1.50	.02
Aldh1a1	Aldehyde dehydrogenase 1 family	2.45	.009
Pdk2	Pyruvate dehydrogenase	1.44	.04

ROS Antioxidant Response

Gene symbol	Gene name	Fold change	*P* value
Sod2	Superoxide dismutase 2, mitochondrial	1.19	.0002
Cat	Catalase	1.27	.0036
Prdx2	Peroxiredoxin 2	1.28	.0048

Apoptotic Response

Gene symbol	Gene name	Fold change	*P* value
Bcl2	B-cell lymphoma 2	1.27	.023
Bax	Bcl2-associated x protein	-1.44	.0018
Trp53	Transformation-related protein p53	-1.87	.00006
Tnfrsf10	Tnfα receptor super family 10; TRAIL	-2.38	.00008
Bnip2	Bcl2 adenovirus interacting protein 2	-1.28	.00025

HIF2-Regulated Targets

Gene symbol	Gene name	Fold change	*P* value
Car9	Carbonic anhydrase 9	2.43	.02
Vegfa	Vascular endothelial growth factor alpha	1.95	.02
Tgfa	Transforming growth factor alpha	1.48	.01

DNA Repair

Gene symbol	Gene name	Fold change	*P* value
Atm	Ataxia telangectasia mutated	-1.85	.0004
Xrcc5	X-ray repair complementing defective repair 5	-2.05	8.0E-05
Chek1	Checkpoint kinase1 homolog	-2.71	.0027
Chek2	Checkpoint kinase 2 homolog	-2.10	.00012
Rad50	Rad50 homolog (S. cerevisiae)	-2.75	1.6E-05
Rad51	Rad51 homolog (S. cerevisiae)	-3.17	.0003
Brca1	Breast cancer 1	-3.36	6.4E-05
Mre11a	Meiotic recombination 11 homolog A	-1.97	.0002

Figure 3. Transcriptional profiling of teratomas reveals altered metabolic reprogramming, HIF2A transcriptional target activation, and suppression of both the DNA damage and apoptotic response in P81S mutants. **A**) Hierarchical clustering of differentially expressed genes from embryonic stem ES) cell teratomas. Stably transfected *Vhl*$^{-/-}$ mouse ES cells expressing wild-type (WT), P81S (both clones represented), or R167Q VHL were injected subcutaneously into the flank region of nude mice and allowed to grow for 4 weeks. RNA was isolated from three to four independent tumors from each genotype and used to perform microarray analysis using the Affymetrix Mouse Gene ST 1.1 whole genome array. Differentially expressed genes between VHL genotypes were determined using Partek Genomics Suite. Statistical significance was determined by analysis of variance; $P \leq .001$. The gene list of 2622 genes was then clustered unsupervised by expression. Log_2 expression color scale: **Red**: upregulated; **Blue**: downregulated. **B**) List of genes differentially regulated exclusively in P81S teratomas. Biological pathway analysis was performed on genes that were differentially regulated in P81S but not in WT or R167Q teratomas. Differentially expressed genes between the apoptosis phenotypes were determined using Partek Genomics Suite. Statistical significance and fold change in expression (antiapoptotic/apoptotic phenotype) was determined by two-sided Student *t* test, $P \leq .05$. **C**) Heat-map showing downregulation of DNA damage response genes in the P81S mutant teratomas compared with WT VHL and R167Q VHL teratomas. Differentially expressed genes were determined Partek Genomics Suite. Statistical significance was determined by analysis of variance, $P \leq .05$. *Atm* = ataxia telengectasia mutated; *Brca1* = breast cancer associated 1; *Chek1* = checkpoint kinase 1; *Chek2* = checkpoint kinase 2; *Mre11a* = meiotic recombination 11 homolog A; *Rad50* = Rad50 homolog A; *Rad51* = Rad51 homolog A; *Xrcc5* = x-ray cross-complimenting 5.

and the proapoptotic genes *Trp53*, *Bax*, *Bnip3*, *and Tnfrsf10* were downregulated only in P81S teratomas, supporting the decreased apoptotic index (Figure 2H). Conversely, expression of *Atm*, a central regulator of the DNA damage response and HIF activation, was suppressed exclusively in the P81S mutant, as were other factors involved in the recognition and response to DNA damage (Figure 3C). This novel finding suggests that there may be a previously unrecognized direct relationship between *Vhl* and *Atm* expression, indicating that suppression of apoptosis within the tumor microenvironment in the P81S mutant may be due to a loss of the DNA damage recognition response.

If metabolic reprogramming and suppression of *Atm* expression leads to attenuation of the P81S mutant apoptotic response, then exposure to a direct-acting exogenous stressor such as radiation should result in decreased Atm phosphorylation and suppression of apoptosis. To test this, teratomas were exposed in vivo to ionizing radiation, revealing a statistically significant reduction in phosphorylated Atm in P81S compared with WT teratomas (mean for P81S = 25.8% vs 54.0% in WT and 47.5% in R167Q; difference = 28.2%; 95% CI = 14.7% to 36.9%; $P < .001$) (Figure 6, A and B), consistent with loss of *Atm* expression in P81S teratomas (Figure 3G). A statistically significant decrease in apoptosis was also observed in P81S VHL teratomas (mean for P81S = 5.9% vs 55.8% in WT and 51.2% in R167Q; difference = 49.9%; 95% CI = 4.7% to 7.1%, $P < .001$) (Figure 6, C and D).

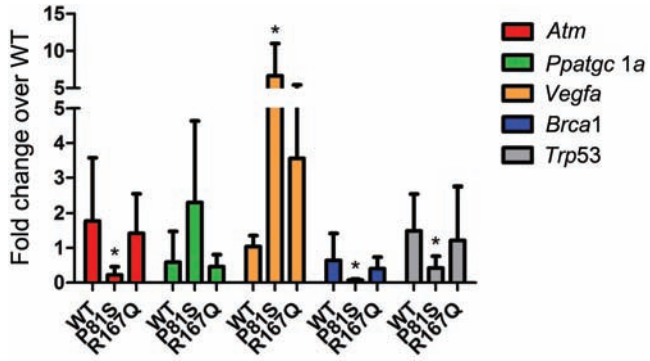

Figure 4. Quantitative reverse-transcription polymerase chain reaction (RT-PCR) validation of differentially expressed genes identified from whole genome arrays on VHL teratomas. Stably transfected *Vhl*$^{-/-}$ mouse embryonic stem (ES) cells expressing wild-type (WT), P81S (both clones represented), or R167Q VHL were injected subcutaneously into the flank region of nude mice and allowed to grow for 4 weeks. RNA was isolated from three to four independent tumors from each genotype and used to perform quantitative RT-PCR analysis on select genes found to be differentially expressed in whole genome microarray experiments by Partek Genomics Suite. Statistical significance was determined by analysis of variance, $*P \leq 0.02$. *Atm* = ataxia telengectasia mutated; *Brca1* = breast cancer associated 1; *Ppargc1a* = peroxisome proliferator alpha receptor gamma isoform c1 alpha; *Trp53* = transformation-related protein p53; *Vegfa* = vascular endothelial growth factor.

Discussion

The data presented herein demonstrate that the TCE-associated P81S *VHL* mutation can dramatically alter growth properties of cells, providing a survival advantage even under environmental stress conditions. Although the mechanism creating this high-frequency somatic mutation is uncertain (1), functional analysis of this unique TCE-associated mutation highlights three important concepts for VHL biology and renal tumorigenesis.

First, although it has been recognized for some time that *VHL* mutations could differentially deploy HIF1A and HIF2A, as well as redirect the transcriptional response, results in this study show that individual mutations such as P81S have effects that are only revealed in the complex in vivo tumor growth environment. It is in the teratoma model that the P81S mutation uniquely displayed potential to traverse tumor initiation and progression, producing highly aggressive in vivo growth. Strikingly, this mutation failed to support an increased angiogenic phenotype that has been characteristic of ccRCC-associated tumors (26) but displayed tissue level hypoxia, which has been characteristically absent in *VHL*-deficient and other *VHL* mutation models (6,18,27). Thus, there is the opportunity with the P81S somatic mutation to produce

A

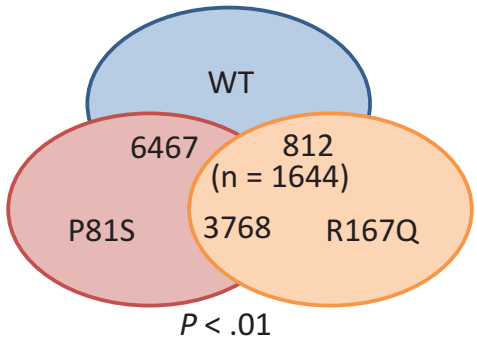

B

Differentially Expressed in Mutant vs WT VHL (n = 1644)

Pathways statistically significantly increased in mutant VHL genotypes (n = 579)

Molecular pathway name	*P* value
Calcium signaling	2.71E-03
PTEN signaling	3.02E-03
Anti-apoptosis signaling	3.57E-03
Decreased permeability transition of mitochondrial membrane	3.14E-04
Hypoxia-inducible factor signaling	1.82E-08

Pathways statistically significantly decreased in mutant VHL genotypes (n = 1065)

Molecular pathway name	*P* value
Assembly of RNA Polymerase II complex	1.91E-04
Estrogen receptor signaling	1.14E-02
Protein ubiquitination signaling	3.09E-02
Nucleotide excision repair pathway	3.96E-02

Figure 5. Transcriptional profiling of teratomas comparing wild-type (WT) vs mutant VHL. **A**) Venn diagram of differentially expressed genes from embryonic stem (ES) cell teratomas. Stably transfected *Vhl*$^{-/-}$ mouse ES cells expressing WT, P81S (both clones represented), or R167Q VHL were injected subcutaneously into the flank region of nude mice and allowed to grow for 4 weeks. RNA was isolated from three to four independent tumors from each genotype and used to perform microarray analysis using the Affymetrix Mouse Gene ST 1.1 whole genome array. Differentially expressed genes between VHL genotypes were determined using Partek Genomics Suite. Statistical significance was determined by Student *t* test and analysis of variance, $P \leq .01$. **B**) List of pathways differentially regulated between both VHL mutants and the WT VHL teratomas. Biological pathway analysis was performed using Ingenuity Pathway Analysis on 1644 genes that were differentially regulated between WT and mutant VHL teratomas; 1065 genes were downregulated and 579 genes were upregulated in mutant VHL teratomas compared with WT. Canonical pathway analysis was measured as a ratio of the number of genes from the dataset that map to a pathway divided by the total number of genes that map to the canonical pathway. Fisher exact test was used to calculate *P* values.

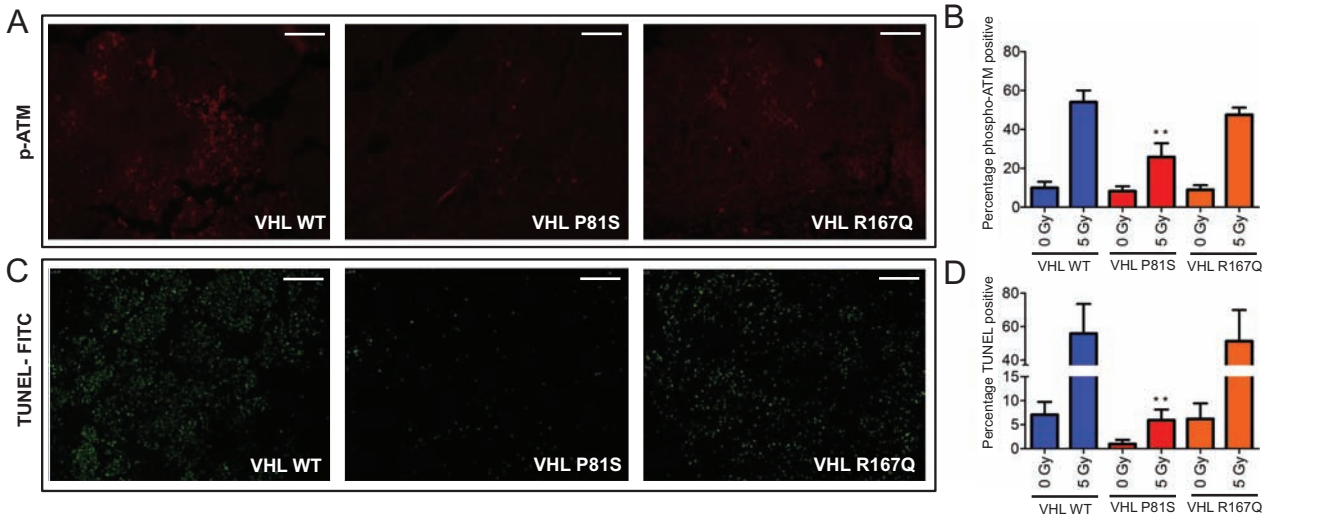

Figure 6. P81S VHL mutant shows reduced phosphorylation of Ataxia Telangiectasia Mutated (ATM) and resistance to ionizing radiation–induced apoptosis. In vivo irradiation of nude mice during teratoma assay of VHL embryonic stem (ES) cell clones. Stably transfected *Vhl*$^{-/-}$ mouse ES cells expressing WT, P81S, or R167Q VHL were injected subcutaneously into the flank region of nude mice and were allowed to grow to a maximum size of 1 cm. Mice were then exposed to a single dose of either 0 Gy or 5 Gy ionizing radiation and killed after 4 and 24 hours. Teratomas were removed and paraffin embedded, and immunohistochemistry was performed on 5-μM sections. **A**) Sections were stained using a primary antibody against phosphorylated-ATM protein at serine 1891 and visualized using a fluorescently conjugated secondary antibody. **Red**: phosphorylated-ATM protein. **B**) Quantification of phosphorylated-ATM in teratomas 4 hours after a single dose of 5 Gy ionizing radiation. Data are mean percentage of phosphorylated-ATM protein ± 95% confidence interval of four random fields at ×100 magnification in three independent tumors per VHL clone. **C**) Sections were stained for apoptosis using a modified terminal deoxynucleotidyl transferase dUTP nick end labeling (TUNEL-FITC) assay with fluorescein isothiocyanate detection. **Green**: cells positive for apoptosis. **D**) Quantification of apoptosis in teratomas 24 hours after a single dose of 5 Gy ionizing radiation. Data are mean percentage of apoptotic cells ± 95% confidence interval of five random fields at ×200 magnification in three independent tumors per VHL clone. *P* values were calculated using analysis of variance, $^{**}P \leq .001$. Scale bars = 200 μm.

phenotypes that are highly influenced by the hypoxic microenvironment of tumor growth.

Second, the P81S mutation is linked to mechanisms that support tumorigenesis by promoting pathways different from the classic glucose metabolism and exuberant angiogenesis that typifies ccRCC (8,26,28,29). In particular, these data demonstrate that VHL-regulated factors can dramatically alter growth properties and are associated with an altered metabolic program. The P81S response signature indicates increased mitochondrial biogenesis, fatty acid oxidation and glutamine synthesis, suggesting that an early step in metabolic reprogramming may be a change in carbon source diversification. In addition to glucose-derived pyruvate, the use of lipids and glutamine provides additional sources of carbon for the trichloroacetic acid (TCA) cycle in the form of acetyl coenzyme A and α-ketoglutarate (11–13). The requirement of energy source diversification is supported by previous studies that have shown that pharmacological inhibition of fatty acid oxidation abolished cellular proliferation and sensitized cells to apoptosis (30) and, further, inhibition of glutaminolysis during hypoxia resulted in loss of cell viability (12). This diversification facilitates "metabolic switching" within the tumor microenvironment during states of environmental stress to support a continuous yield of reducing equivalents for oxidative phosphorylation, aiding tumor survival.

Third and finally, P81S teratomas gained a growth advantage resulting from apoptotic resistance rather than enhanced proliferation, raising the threshold of sensitivity to endogenous and exogenous stressors. Transcriptomic analysis suggested that a key component of this growth advantage is a disabling of the DNA damage response through suppression of DNA damage recognition and repair proteins. The loss of these genoprotective mechanisms was associated with decreased phosphorylation of Atm 4 hours after irradiation and a blunted apoptotic response at 24 hours after irradiation. This highlights a previously uncharted intersection of VHL programming and the DNA damage response, which, in the case of the P81S mutation, produces a highly advantageous growth environment.

Functional analysis of the unique TCE-associated P81S VHL mutant supports a new model whereby the VBC complex is disrupted and stabilizes HIF during normal oxygen conditions, thus priming tumor cells for adaptation when challenged by a hypoxic tumor microenvironment (Figure 7). To continue proliferation and avoid apoptotic stress signals, the P81S mutant likely initiates an adaptive environmental stress response by pleiotropic effects. By modulating energy metabolism genes, upregulating radical scavenging antioxidant genes, and downregulating key DNA damage response and proapoptotic genes, the P81S mutant is able to suppress apoptotic signals and continue proliferating within a hypoxic microenvironment, even resisting irradiation-induced apoptosis. These findings are relevant for understanding how mutations in *VHL* could promote tumorigenesis by driving metabolic diversification, demonstrating a class of *VHL* mutations for which tumors may be inherently resistant to radiation and antiangiogenic therapies and which may require alternate targeting strategies.

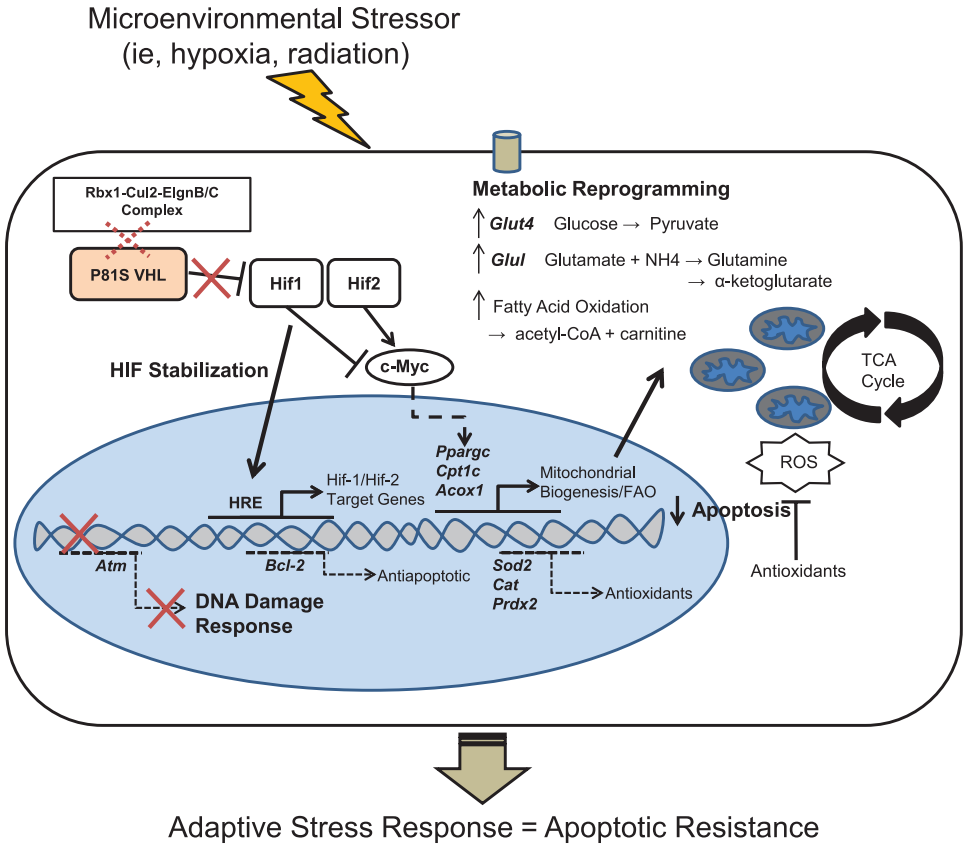

Figure 7. Schematic of model proposing mechanism of altered stress response and apoptotic resistance of P81S VHL mutant. P81S VHL mutation allows hypoxia-inducible transcription factor family (HIF) stabilization and transcriptional activation during normal oxygen conditions, creating a state of chronic "pseudo-hypoxic" signaling within the cell. HIF activation and transcriptional signaling in the presence of oxygen primes tumor cells for adaption when challenged by a hypoxic tumor microenvironment. The transcriptional data suggest that the initial step in metabolic reprogramming may be a change in carbon source diversification. In addition to glucose-derived pyruvate, the use of lipids and glutamine provides additional sources of carbon for the tricarboxylic acid cycle (TCA) cycle in the form of acetyl coenzyme A and α-ketoglutarate. This diversification would then facilitate "metabolic switching" within the proliferative tumor microenvironment to support a continuous yield of reducing equivalents for oxidative phosphorylation. As a compensatory mechanism to prevent reactive oxygen species (ROS)-induced damage, antioxidant genes are upregulated and proapoptotic genes are suppressed, along with the DNA damage response, resulting in an apoptotic-resistance phenotype secondary to changes in metabolism. *Acox*, acyl-Coenzyme A oxidase; *Atm*, ataxia telangiectasia mutated; *Bcl2*, b-cell lymphoma factor 2; *Cat*, catalase; *Cpt1c*, carnitine palmitoyltransferase; *Cul2*, cullin-2; *Elgnb*, elongin B; *Eglnc*, elongin C; FAO, fatty acid oxidation; *Glul*, glutamine synthase; *Glut4*, glucose transporter 4; *Hif1*, hypoxia-inducible factor isoform 1; *Hif2*, hypoxia-inducible factor isoform 2; HRE, hypoxia response element; *Ppargc*, peroxisome proliferator alpha receptor gamma isoform c1 alpha; *Prdx2*, peroxiredoxin 2; *Rbx1*, ringbox 1; *Sod2*, mitochondrial superoxide dismutase.

This study had some limitations. First, we used the in vivo teratoma assay to perform a comparative analysis of mouse embryonic stem cells expressing human gene variants, and although this system has successfully modeled several human VHL mutation-associated phenotypes (18), the tumor microenvironmental cues are endogenously derived. The selective growth pressure and response may be altered in a single mutated cell among surrounding terminally differentiated cells. Second, the metabolic reprogramming observed in transcriptional profiles of P81S VHL teratomas shows clear translational potential and is an exemplar of the metabolic changes that commonly occur in human renal tumors. Future studies should be aimed at the functional analysis of these metabolic alterations, including quantitative physiological measurements of mitochondrial function and fatty acid metabolism. Third, the evaluation of the TCE exposure–associated P81S *VHL* mutation suggests a potential mechanism for tumor promotion and does not elucidate the mode of action for TCE exposure–associated *VHL* mutagenesis. There is a critical need for additional biologically based exposure models to examine the conditions necessary for exposure-induced renal carcinogenesis. Fourth, although VHL has several cellular functions, its modulation of ATM-mediated DNA damage response suggests it plays a role in the DNA damage response network, and additional studies will be required to elucidate this newly identified relationship.

In summary, the TCE-associated somatic *VHL* mutation presents a high-risk allele for clonal expansion and highlights several new features of *VHL*-related tumorigenesis that are often overshadowed by effects on glycolysis and tumor angiogenesis, commonly associated with *VHL* loss. Although numerous reports have linked HIF activation to metabolic reprogramming (28,31), this is the first report connecting a particular *VHL* mutation to cellular metabolic regulation and ATM damage response and demonstrating that microenvironmental cues likely factor heavily on in vivo phenotypes.

References

1. Brauch H, Weirich G, Hornauer MA, et al. Trichloroethylene exposure and specific somatic mutations in patients with renal cell carcinoma. *J Natl Cancer Inst*. 1999;91(10):854–861.
2. Brauch H, Weirich G, Klein B, et al. VHL mutations in renal cell cancer: does occupational exposure to trichloroethylene make a difference? *Toxicol Lett*. 2004;151(1):301–310.
3. Ivan M, Kondo K, Yang H, et al. HIFalpha targeted for VHL-mediated destruction by proline hydroxylation: implications for O2 sensing. *Science*. 2001;292(5516):464–468.
4. Kaelin WG Jr. The von Hippel-Lindau protein, HIF hydroxylation, and oxygen sensing. *Biochem Biophys Res Commun*. 2005;338(1):627–638.
5. Hacker KE, Lee CM, Rathmell WK. VHL type 2B mutations retain VBC complex form and function. *PLoS One*. 2008;3(11):e3801.
6. Lee CM, Hickey MM, Sanford CA, et al. VHL Type 2B gene mutation moderates HIF dosage in vitro and in vivo. *Oncogene*. 2009;28(14):1694–1705.
7. Stebbins CE, Kaelin WG, Jr., Pavletich NP. Structure of the VHL-ElonginC-ElonginB complex: implications for VHL tumor suppressor function. *Science*. 1999;284(5413):455–461.
8. Pinthus JH, Whelan KF, Gallino D, et al. Metabolic features of clear-cell renal cell carcinoma: mechanisms and clinical implications. *Can Urol Assoc J*. 2011;5(4):274–282.
9. Warburg O. On the origin of cancer cells. *Science*. 1956;123(3191):309–314.
10. Menendez JA, Lupu R. Fatty acid synthase and the lipogenic phenotype in cancer pathogenesis. *Nat Rev Cancer*. 2007;7(10):763–777.
11. Liu Y. Fatty acid oxidation is a dominant bioenergetic pathway in prostate cancer. *Prostate Cancer Prostatic Dis*. 2006;9(3):230–234.
12. Wise DR, Ward PS, Shay JE, et al. Hypoxia promotes isocitrate dehydrogenase-dependent carboxylation of alpha-ketoglutarate to citrate to support cell growth and viability. *Proc Natl Acad Sci U S A*. 2011;108(49):19611–19616.
13. Le A, Lane AN, Hamaker M, et al. Glucose-independent glutamine metabolism via tca cycling for proliferation and survival in B cells. *Cell Metab*. 2012;15(1):110–121.
14. Gaglio D, Metallo CM, Gameiro PA, et al. Oncogenic K-Ras decouples glucose and glutamine metabolism to support cancer cell growth. *Mol Syst Biol*. 2011;7:523.
15. Montopoli M, Bellanda M, Lonardoni F, et al. "Metabolic reprogramming" in ovarian cancer cells resistant to cisplatin. *Curr Cancer Drug Targets*. 2011;11(2):226–235.
16. Cam H, Easton JB, High A, et al. mTORC1 signaling under hypoxic conditions is controlled by ATM-dependent phosphorylation of HIF-1alpha. *Mol Cell*. 2010;40(4):509–50.
17. Kim SG, Choo AY, Blenis J. ATM: Promoter of metabolic "cost" reduction and "savings" usage during hypoxia through mTORC1 regulation. *Mol Cell*. 2010;40(4):501–502.
18. Rathmell WK, Hickey MM, Bezman NA, et al. In vitro and in vivo models analyzing von Hippel-Lindau disease-specific mutations. *Cancer Res*. 2004;64(23):8595–8603.
19. Livak KJ, Schmittgen TD. Analysis of relative gene expression data using real-time quantitative PCR and the 2(-Delta Delta C(T)) method. *Methods*. 2001;25(4):402–408.
20. Edgar R, Domrachev M, Lash AE. Gene Expression Omnibus: NCBI gene expression and hybridization array data repository. *Nucleic Acids Res*. 2002;30(1):207–210.
21. Covello KL, Simon MC, Keith B. Targeted replacement of hypoxia-inducible factor-1alpha by a hypoxia-inducible factor-2alpha knock-in allele promotes tumor growth. *Cancer Res*. 2005;65(6):2277–2286.
22. Santamaria G, Martinez-Diez M, Fabregat I, et al. Efficient execution of cell death in non-glycolytic cells requires the generation of ROS controlled by the activity of mitochondrial H+-ATP synthase. *Carcinogenesis*. 2006;27(5):925–935.
23. Vander Heiden MG, Cantley LC, Thompson CB. Understanding the Warburg effect: the metabolic requirements of cell proliferation. *Science*. 2009;324(5930):1029–1033.
24. Sasabe E, Tatemoto Y, Li D, et al. Mechanism of HIF-1alpha-dependent suppression of hypoxia-induced apoptosis in squamous cell carcinoma cells. *Cancer Sci*. 2005;96(7):394–402.
25. Cuisnier O, Serduc R, Lavieille JP, et al. Chronic hypoxia protects against gamma-irradiation-induced apoptosis by inducing bcl-2 up-regulation and inhibiting mitochondrial translocation and conformational change of bax protein. *Int J Oncol*. 2003;23(4):1033–1041.
26. Carmeliet P, Dor Y, Herbert JM, et al. Role of HIF-1alpha in hypoxia-mediated apoptosis, cell proliferation and tumour angiogenesis. *Nature*. 1998;394(6692):485–490.
27. Mack FA, Rathmell WK, Arsham AM, et al. Loss of pVHL is sufficient to cause HIF dysregulation in primary cells but does not promote tumor growth. *Cancer Cell*. 2003;3(1):75–88.
28. Semenza GL. HIF-1: upstream and downstream of cancer metabolism. *Curr Opin Genet Dev* .2010;20(1):51–56.
29. Sudarshan S, Karam JA, Brugarolas J, et al. Metabolism of kidney cancer: from the lab to clinical practice. *Eur Urol*. 2012;63(2):244–251.
30. Samudio I, Harmancey R, Fiegl M, et al. Pharmacologic inhibition of fatty acid oxidation sensitizes human leukemia cells to apoptosis induction. *J Clin Invest*. 2010;120(1):142–156.
31. Kroemer G, Pouyssegur J. Tumor cell metabolism: cancer's Achilles' heel. *Cancer Cell*. 2008;13(6):472–482.

Funding

This work was supported by the North Carolina Clinical and Translational Sciences Institute; a Howard Hughes Medical Institute Med-into-Grad Fellowship; and the National Institutes of Health (grants UL1 TR000083, UL1 RR025747, P30 CA016086, R01 CA121781, and R01 CA105417).

Notes

The study sponsor did not participate in the collection, analysis or interpretation of the data, writing of the manuscript, nor the decision to submit the manuscript for publication.

We would like to acknowledge assistance from the UNC Lineberger Cancer Center Animal Studies, Genomics, and Sequencing core facilities and to thank Shelly West and Dr Jon Serody for assistance in radiation experiments.

Affiliations of authors: Department of Genetics, North Carolina State University, Raleigh, NC (MCD, DWT); Department of Genetics (WKR) and Lineberger Cancer Center, University of North Carolina, Chapel Hill, NC (WKR, DWT).